

# ULRR

## Micro-mixing characteristics of a pinched-tube, a fluidic oscillator and a vortex-based cavitation device#

Item Type	Article
Authors	Joshi, Amol N.;Ganjare, Amol;Hudson, Sarah;Ranade, Vivek
Citation	Chemical Engineering Journal 515, 163657
Publisher	Elsevier
Download date	2026-06-17 17:05:46
Item License	<a href="https://creativecommons.org/licenses/by-nc-sa/4.0/">https://creativecommons.org/licenses/by-nc-sa/4.0/</a>
Link to Item	<a href="https://doi.org/10.34961/researchrepository-ul.29245478">https://doi.org/10.34961/researchrepository-ul.29245478</a>



# Micro-mixing characteristics of a pinched-tube, a fluidic oscillator and a vortex-based cavitation device<sup>☆</sup>

Amol N. Joshi<sup>a,b</sup>, Amol V. Ganjare<sup>a,b</sup>, Sarah Hudson<sup>b,c</sup>, Vivek V. Ranade<sup>a,b,c,\*</sup>

<sup>a</sup> Multiphase Reactors and Intensification Group, Bernal Institute, University of Limerick, Limerick, Ireland

<sup>b</sup> Department of Chemical Sciences, Bernal Institute, University of Limerick, Limerick, Ireland

<sup>c</sup> SSPC Science Foundation Ireland Research Centre for Pharmaceuticals, Bernal Institute, University of Limerick, Limerick, Ireland

## ARTICLE INFO

### Keywords:

Engulfment model  
Fluidic devices  
Villermaux Dushman reaction  
Energy dissipation rate

## ABSTRACT

Micro-mixing plays a crucial role in controlling performance and quality of products from anti-solvent crystallization, reactive precipitation and nanoparticle synthesis. In this work, micro-mixing was characterised using the Villermaux Dushman iodide-iodate reactions in three fluidic devices namely a pinched-tube, a fluidic oscillator and a vortex-based cavitation device operated in a loop configuration. A three-environment engulfment model was developed to simulate mixing and reactions in these devices operated in a flow loop. The loop was operated at different flow rates to cover a broad range of energy dissipation rates ( $\epsilon = \sim 10^{-1}$ – $10^4$  W/kg) with the three devices. The considered fluidic devices exhibited micro-mixing times in the range of 28–160 ms. The micro-mixing times estimated from the engulfment model were found to be proportional to  $\epsilon^{-0.17}$ . Among the investigated devices, the fluidic oscillator had the lowest micro-mixing time of  $\sim 28$  ms. The pinched tube exhibited a micro-mixing time in the range of 30–74 ms while the vortex-based cavitation device exhibited a micro-mixing time in the range of 33–80 ms before the inception of cavitation. For the conditions where cavitation occurred in the vortex-based cavitation device, the usual method of estimation of micro-mixing time was not suitable since oxidising radicals generated by cavitation interfere with the Villermaux Dushman reactions. The presented model, data and discussion will be useful for selecting appropriate fluidic devices for mixing applications and further work on characterising mixing in cavitation devices.

## 1. Introduction

Mixing plays an important role in controlling the overall performance and product quality in a variety of industrially important processes. Realising mixing on a molecular scale is essential for any process operation such as reactions or anti-solvent crystallisation/precipitation which involves mixing of two process streams. Mixing on the molecular scale occurs via the continuous reduction of scale and intensity of mixing [1–4]. Depending on the length and time scales of mixing, it is broadly categorised as macro-mixing (governed by convection and mean flow), meso-mixing (governed by turbulence and shear at intermediate scales) and micro-mixing (governed by engulfment and molecular diffusion). In this work, we have characterised micro-mixing in three fluidic devices namely pinched-tube, fluidic oscillator and vortex-based cavitation device operated in a loop configuration.

Several types of mixers are used in practice including ubiquitous

stirred vessels [5–10]. There is an increasing trend to develop and use fluidic devices offering intensified mixing as “enabling technologies” [11]. A large variety of fluidic devices without any moving parts have been developed for a variety of applications [12–17]. One of the most striking applications of such devices was the production of mRNA-lipid nanoparticles (LNPs) vaccine during the COVID-19 pandemic by Pfizer-BioNTech that aimed to reduce the risks related to the virus. Pfizer-BioNTech [18] produced the mRNA encapsulated LNPs (more than three billion doses) by rapidly mixing two streams – an organic solvent containing lipids and antisolvent containing mRNA in a confined impinging jet mixer. The devices without any moving parts (sometimes called passive devices) which require less maintenance and facilitate number up (operating multiple devices in parallel) are gaining increased attention. For widening the application horizons of such fluidic devices without moving parts, it is essential to characterise their micro-mixing characteristics.

Relatively few studies characterise micro-mixing performance and

<sup>☆</sup> This article is part of a special issue entitled: ‘ISCRE 28’ published in Chemical Engineering Journal.

\* Corresponding author at: Multiphase Reactors and Intensification Group, Bernal Institute, University of Limerick, Limerick, Ireland.

E-mail address: [Vivek.Ranade@ul.ie](mailto:Vivek.Ranade@ul.ie) (V.V. Ranade).

**Nomenclature**

$\tau$	Mean residence time in the reactor (s)
$t_{micro}$	Micro-mixing time (s)
$t_{macro}$	Macro-mixing time (s)
$t_R$	Reaction time scale (s)
$E$	Engulfment rate (inverse of micro-mixing time) ( $s^{-1}$ )
$V$	Total reactor volume ( $m^3$ )
$C_{kj}$	Concentration of species $k$ in environment $j$ ( $mol\ L^{-1}$ )
$C_{k_o}$	Outlet concentration of species $k$ ( $mol\ L^{-1}$ )
$T$	Temperature (K)
$\Delta t$	Time step for engulfment model transient differential equations (s)
$Re$	Reynolds number

**Greek Letters**

$\varepsilon$	Energy dissipation rate ( $W\ kg^{-1}$ )
$\epsilon$	Molar extinction coefficient of triiodide ( $M^{-1}\ cm^{-1}$ )
$\rho$	Density ( $kg\ m^{-3}$ )
$\mu$	Dynamic viscosity ( $Pa\ s$ )
$\nu$	Kinematic viscosity ( $m^2s^{-1}$ )

the majority of the micro-mixing studies focus on microfluidic devices. Table 1 shows the different devices that have been studied for micro-mixing performance. Microfluidic devices exhibit a better micro-mixing performance due to smaller diffusion length scales compared to conventional stirred reactors [19]. However, these devices lack scalability due to low throughputs of  $\mu L\ min^{-1}$  to a few  $mL\ min^{-1}$ , expensive fabrication and limitations on process conditions [20]. Thus, there is a need to develop fluidic devices that are scalable, have high throughput capacities and exhibit the same or better micro-mixing characteristics as that of microfluidic devices. Despite the promising results obtained with pinched-tube [12,14], fluidic oscillators [16,21,22] and vortex-based cavitation devices [23–25] for a variety of applications, the micro-mixing performance of these devices has not yet been characterised. The present work attempts to bridge this gap by characterising micro-mixing times in three fluidic devices. These devices were studied using the loop configuration (discussed later in Section 2) so as to realise a wide range of energy dissipation rates ( $10^{-1} - 10^4\ W/kg$ ).

In a pinched-tube, the pinching produces alternate converging and diverging sections that alternately accelerate and decelerate the fluid flow, inducing changes in the velocity and flow directions resulting in turbulence and enhanced mixing [12]. In a fluidic oscillator when a liquid jet comes out of a nozzle into a free surrounding, it entrains and mixes with fluids in the surrounding of the jet. The presence of a surface close to the jet, limits the entrainment in that region. As flow accelerates to balance the momentum transfer, a pressure difference is generated and eventually the jet attaches to the surface. This phenomenon generates self-sustaining oscillations of the jet of fluid that induces enhanced mixing [21]. A vortex diode is a cavitating device which generates cavities when a liquid passes through a low-pressure region; these cavities grow, oscillate and finally collapse in a high-pressure region [23]. The oscillation and subsequent collapse of cavities creates high shear microjets creating turbulence and hence intensify mixing [26]. In this work, micro-mixing in these three devices is characterised using fast competitive reactions, as they are sensitive to mixing at molecular scales.

Over the past few decades, two reaction schemes have mainly been studied for micro-mixing characterization – Bourne reactions and Villermaux Dushman iodide-iodate reactions [27–33]. Considering the availability of the relevant kinetic data, ease of analysis of the product of interest using UV-Visible Spectroscopy and, ambient pressure and



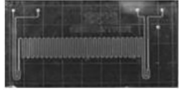

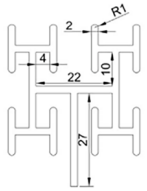
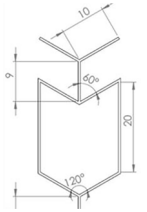
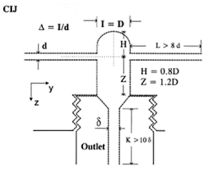
temperature conditions, the Villermaux Dushman iodide-iodate reactions were selected in this work to determine micro-mixing times. The yield of undesired product is used as a measure of micro-mixing – higher yield of undesired products indicates lower micro-mixing (or longer micro-mixing time). A mixing model is needed for relating experimentally measured yield of undesired product to quantitative value of micro-mixing time. The most commonly used models for simulating micro-mixing include the engulfment model (E-model) [34,35], the interaction by exchange with the mean (IEM) model [36], engulfment deformation diffusion (EDD) model [37] and the incorporation model [38]. These models are primarily developed for conventional semi-batch reactors. The previously published models are not directly applicable for characterising micro-mixing for a loop configuration used in this work. The classical engulfment model of Baldyga and Bourne [35] was therefore extended to simulate micro-mixing in a loop configuration as a three-environment engulfment model. Mixing through a straight tube with recirculation was selected as the base case and micro-mixing time in the three fluidic devices – pinched-tube, fluidic oscillator and vortex diode was determined. These devices and envisaged operating parameters encompass a wide range of energy dissipation rates,  $\varepsilon$  ( $\sim 10^{-1} - 10^4\ W/kg$ ). An anomalous trend in the variation of the micro-mixing time with energy dissipation rate was observed in the presence of cavitation (in the vortex-based cavitation device). Control experiments were performed to quantify the potential oxidation of iodide by hydroxyl radicals generated by cavitation [39] which may interfere with the reaction pathways and yield. The micro-mixing characteristics of the considered three devices were compared with the other fluidic devices. The presented results will be useful for selecting appropriate mixing devices for desired applications.

**2. Experimental****2.1. Experimental setup and operation**

The aim of this work was to characterise micro-mixing of pinched-tube, fluidic oscillator and vortex-based cavitation device over a range of energy dissipation rates. It should be noted that there is a minimum flow rate requirement to initiate jet oscillations and mixing in fluidic oscillator [21]. The flow rate through the pinched-tube and vortex-based cavitation device also needs to be quite high ( $0.5 - 2\ L\ min^{-1}$ ) to achieve the desired energy dissipation rates. It is not practically feasible to carry out Villermaux Dushman reactions with such a high flow rate of reactants to achieve high energy dissipation rates. Secondly, more often than not, these devices are used with re-circulation [13,50,51]. Therefore, in this work, micro-mixing of these devices was characterised by operating these devices with a re-circulation (hence forth referred as a loop configuration). The schematic of experimental setup is shown in Fig. 1. This loop configuration allowed variation of energy dissipation rates without changing the net flow rates of reactants.

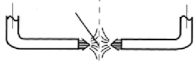
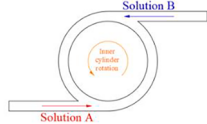
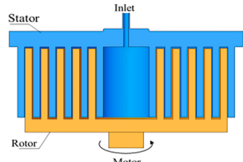
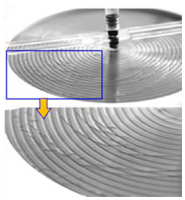
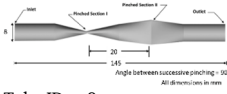
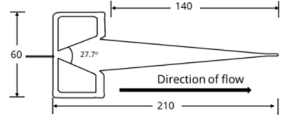
Two reactant streams are needed for carrying out Villermaux Dushman reactions (discussed in Section 2.2). A double syringe pump (Harvard Apparatus PHD ULTRA 70–3005) was used with two 60 mL syringes to deliver these two reactant streams with equal volumetric flow rates ( $10\ mL\ min^{-1}$ ) to the fluidic device in the loop configuration. The two inlet streams were passed to a four-way junction (internal diameter = 4 mm) which then connects to the inlet of the fluidic devices. A peristaltic pump (Longer make – WT6002J) was used for maintaining the flow of the recirculation loop ( $0.5 - 2\ L\ min^{-1}$ ). One outlet stream was drawn from the recycle loop. The flow rate of the outlet was self-maintained as the volume of the loop was fixed (22 mL). The recirculation flow rate in the loop was varied to achieve different rates of energy dissipation within the flow loop. Samples were collected from the outlet once the steady state was achieved (typically after four residence times). Briefly, samples were collected after three, four and five residence times where residence time is the ratio of total volume of the system to the total inlet volumetric flow rate. There was no change in the

**Table 1**  
State-of-the-art on micro-mixing performance of different devices.

Device/mixer	Device design	Studies performed	Key results	Comments
Tee-mixer 90° bends (Tee90) [30]	 Width = 1 mm, depth = 1 mm, total length = 18 cm	Micro-mixing with Interaction by Exchange with the Mean (IEM) model.	Micro-mixing time of 12–100 ms. $t_{micro} \propto \epsilon^{-0.45}$	Micro-mixing time shows an increase when Re is between 500 and 600.
Tee-mixer [40]	 OD = 1/16", volume = 0.067 mL; OD = 1/8", volume = 0.27 mL	Re = 100–600. Micromixing with IEM model. Flow rate = 1–20 mL min <sup>-1</sup>	Micro-mixing time of 32 ms and 199 ms for 1/16" and 1/8" tee-mixer respectively at 20 mL min <sup>-1</sup> . $t_{micro} = 1.6X_S$ for set 2B	IEM model with complete dissociation and step wise dissociation of sulphuric acid. No difference observed.
Commercial chip reactors (KiloFlow and Labtrix) [41]	 Volume = 10–19.5 μL	Micro-mixing with Incorporation model. Re = 40–160	$t_{micro} = 0.08X_S$ for set 2B. Micro-mixing time of about 1 ms.	Low micro-mixing time due to chaotic advection compared to conventional tubular reactors.
Syrris micromixer and Syrris plate microchannel [42]	 Volume = 6.25 μL Mixing channel dimensions = 50 x 125 μm	Micro-mixing with IEM model. Flow rate = 0.1–4 mL min <sup>-1</sup> $\epsilon_{micromixer} = 1-6$ W/kg $\epsilon_{plate} = 1-8$ W/kg	Micro-mixing time of 40–60 ms over the range of epsilon studied. $t_{micro} \propto \epsilon^{-0.1}$	Dispersion number < 0.01. Micro-mixing time decreased when $\epsilon$ increased from 1 to 2 W/kg and then levelled off for higher $\epsilon$ . Micro-mixing time does not solely depend on pressure drop and $\epsilon$ . It depends on various 'design factors' of the devices.
Multichannel micromixer heat exchanger (M1 and M2) [43]	 M1: diameter = 1 mm, volume = 1.27 mL M2: diameter = 2 mm, volume = 6.07 mL	Micro-mixing with IEM model. [NaOH] = 0.125 [H <sub>3</sub> BO <sub>3</sub> ] = 0.25 [KI] = 0.0116 [KIO <sub>3</sub> ] = 0.00233 [H <sup>+</sup> ] = 0.072 (concentrations in mol L <sup>-1</sup> ) Flow rate = 600–1200 mL min <sup>-1</sup> , $\epsilon = 4-3000$ W/kg	$t_{micro,M1} = 8$ ms $t_{micro,M2} = 15$ ms $t_m = 2.55X_S$ M1: $t_{micro} \propto \epsilon^{-0.13}$ M2: $t_{micro} \propto \epsilon^{-0.22}$	Decreasing the dimensions of mixing device by half, the micro-mixing time reduced by half while maintaining the same $\epsilon$ . $t_{micro}$ is not solely a function of $\epsilon$ .
Multistage Y-A shaped microreactor (YA) [44]	 Channel diameter = 500 μm Y-angle = 60° Length of 1 section = 20 mm	Micromixing time determined using mixing time-absorbance correlation given by Commenge and Falk [30] Flow rate = 1–10 mL min <sup>-1</sup>	Micro-mixing time of about 40 ms at the highest flow rate. $t_{micro} = 4X_S$ for set 2B	The micro-mixing time decreased did not level off. There is a possibility of it to decrease further if flow rates above 10 mL min <sup>-1</sup> are tested. Flow splitting and recombination is responsible for low micro-mixing times at such low flow rates.
Confined impinging jet mixer (CIJ) [45]	 Nozzle diameter (d) = 0.5 mm Chamber diameter (D) = 2.38 mm Distance between impinging zone and chamber = 1.2 D	Micro-mixing (competitive reactions of neutralization and dimethoxypropane acid hydrolysis) Scaling-model based on momentum diffusion from Kolmogorov length scale. Re = 100–3000	Micro-mixing time of 9.5 ms at Re of 3000. $t_{micro} \propto u^{-1.5}$ u: average velocity of stream	—

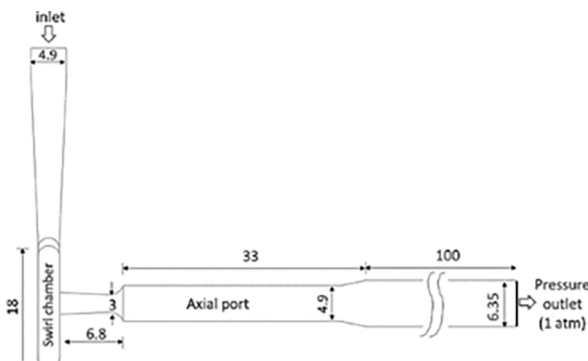
(continued on next page)

Table 1 (continued)

Device/mixer	Device design	Studies performed	Key results	Comments
Impinging Jet Mixer (IJM) [46]	 Nozzle diameter = 1 mm	Micro-mixing with incorporation model.  Flow rate = 1–10 mL s <sup>-1</sup>  $\epsilon = 2\text{--}20$ W/kg	Micro-mixing time of about 4 ms at $\epsilon$ of 20 W/kg.  Same micro-mixedness ratio at higher flow rates.  $t_{\text{micro}} \propto \epsilon^{-0.5}$	Mixing volume is concentrated in a small area of impinging zone.  Experimental energy dissipation rates results showed good agreement with the ones obtained from k- $\epsilon$ model (CFD).
Annular rotating flow mixer (ARFM) [47]	 Inner cylinder diameter = 12 mm Outer cylinder diameter = 14–17 mm Volume = 1.71–4.78 mL Tangential feed inlet	Micro-mixing with Incorporation model.  Flow rate = 9–45 mL min <sup>-1</sup> Rotation speed = 0–5400 rpm Re = 100–500 $\epsilon = 100\text{--}4000$ W/kg	Micro-mixing time of the order of 0.1 ms over $\epsilon$ range of 100–1000 W/kg.  $t_{\text{micro}} = 0.072X_S^{1.08}$ for set 1C  $t_{\text{micro}} \propto \epsilon^{-0.52}$	Device with moving parts.  Micro-mixing time decreased with an increase in $\epsilon$ till 1500 W/kg after which it showed an increase in micro-mixing time which was attributed to $\epsilon$ in the entrainment region.
Microannular rotating bed (MARB) [48]	 Stator diameter = 220 mm Rotor diameter = 204 mm Annular gap = 1 mm	Micro-mixing with incorporation model.  Flow rate = 0.6–6 L min <sup>-1</sup> $\epsilon = 50\text{--}4000$ W/kg  Flow rate ratio of buffer to acid = 10.  [H <sub>3</sub> BO <sub>3</sub> ] = 0.1818 [K <sup>+</sup> ] = 0.01167 [KIO <sub>3</sub> ] = 0.00233 [H <sup>+</sup> ] = 0.45 (concentrations in mol L <sup>-1</sup> )	Micro-mixing time of 0.1–1 ms.  $t_{\text{micro}} = 0.29X_S^{1.07}$	Pressure drop was not considered in energy dissipation rate. Only energy input for rotation was used.  Slope of $t_{\text{micro}}$ vs $\epsilon$ was significantly higher (1.4) compared to standard correlations (0.45–0.5). It was attributed to higher energy efficiency of MRB.
Impinging jet flow on spinning disk reactor (structured surface) (IJSDR) [49]	 Disk diameter = 200 mm Depth of grooves = 0.2 mm Width of grooves = 2 mm	Surface of spinning disk–radial and concentric grooves.  Micro-mixing with incorporation model. Rotating speed = 300–1500 rpm.	Micro-mixing time in the range 0.04–2.19 ms.  $t_{\text{micro}} \propto \epsilon^{-0.374}$	Device with moving parts.  Micro-mixing time decreased with increase in $\epsilon$ and levelled off at $\epsilon > 2000$ W/kg.
Pinched-tube (Present work)	 Tube ID = 8 mm R/a = 4 Total length = 145 mm Angle between successive pinches = 90° Volume = 7 mL	Micro-mixing with three-environment engulfment model.  Re = 1300–5300 $\epsilon = 0.3\text{--}12$ W/kg	Micro-mixing time was estimated using the relation $t_{\text{micro}} = 3.4X_S$ for set 2B  Micro-mixing time in the range 30–70 ms	–
Fluidic oscillator (Present work)	 Hydraulic diameter = 2.25 mm Total length = 240 mm Distance from inlet to backflow limbs = 70 mm Diverging angle = 27.7° Volume = 7.5 mL	Micro-mixing with three-environment engulfment model. Re = 4700–14,000 $\epsilon = 12\text{--}220$ W/kg	Micro-mixing time in the range of 28–42 ms	–

(continued on next page)

Table 1 (continued)

Device/mixer	Device design	Studies performed	Key results	Comments
Vortex-based cavitation device (vortex diode)  (Present work)	 <p>Throat diameter = 3 mm Length of swirl chamber = 18 mm Volume = 0.7 mL</p>	<p>Micro-mixing with three-environment engulfment model.</p> <p><math>Re = 700\text{--}14,000</math> <math>\epsilon = 2\text{--}9600 \text{ W/kg}</math></p>	Micro-mixing time in the range of 33–80 ms.	Oxidation of iodide from the feed due to cavitation effect needs to be accounted.

\*All the studies are with Villermaux Dushman reactions unless otherwise specified. \*For concentration set 2B and 1C refer to Supplementary Information S5. \*All figures produced with permissions from Ref. 30 and [40-49].

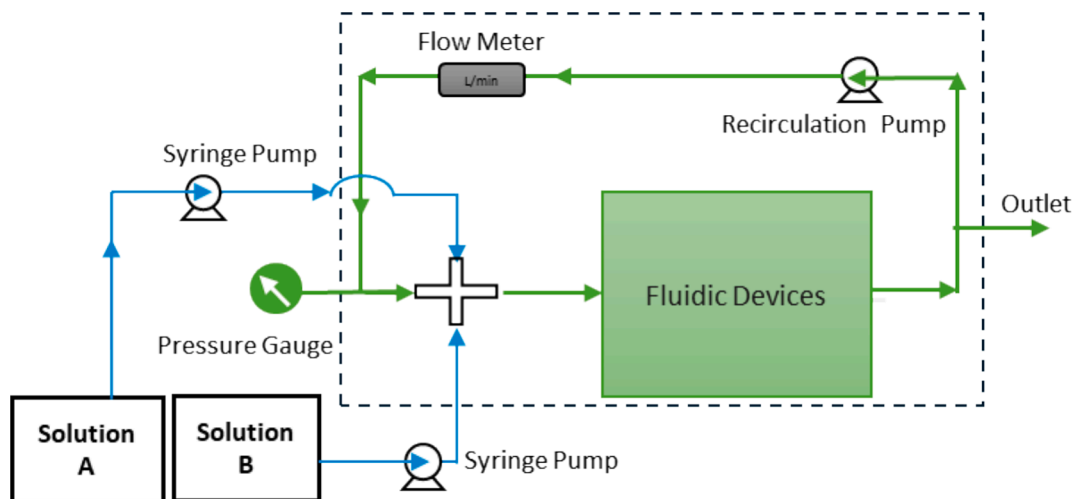


Fig. 1. Schematic of the experimental setup.

product concentration after four residence times confirming that the steady state was reached. Convenient arrangements were made to replace the different fluidic devices in the setup. These arrangements did not disturb the other sections in the experimental setup. Three fluidic devices – pinched-tube, fluidic oscillator and vortex diode along with a straight tube (25 cm long) as a base case were studied for the micro-mixing. The dimensions of the fluidic devices and tubing used in the set-up are included in Supplementary Information (see Section S4). Dimensions were verified by the suppliers as well as through measurements of key characteristics in the lab. The characteristic length scales

**Table 2**  
Characteristic length scales and characteristic area for devices under consideration.

Device	Characteristic length scales ( $d_c$ ) (mm)	Characteristic area ( $A_c$ ) ( $\text{mm}^2$ )
Straight tube	4.0	12.56
Pinched-tube	8.0	50.27
Fluidic oscillator	2.25	3.98
Vortex-based cavitation device	3.0	7.07

and areas for the pinched-tube, fluidic oscillator and vortex-based cavitation device used in this work are listed in Table 2. Vortex diode and fluidic oscillator were fabricated using CNC machines and had very small manufacturing tolerances. The pinched-tube used in this work was fabricated by taking a commercial straight tube and pinching it in an internal workshop. It was not possible to measure dimensions of the pinched section very accurately and the dimensions mentioned in the Supplementary Information may be considered with an accuracy of  $\pm 5\%$ . Before performing the micro-mixing reactions in the fluidic devices, the hydrodynamic characteristics – pressure drop and rate of energy dissipation were studied.

The pressure drops across all the different fluidic devices were measured independently with water instead of reactant streams using a digital pressure meter (Digitron 2000P Differential Pressure Meter) having a range of 0 – 700 kPa (accuracy = 0.1 %). The flow rates were monitored using a digital flow meter (Krohne make – AF-E 400). The pressure drop measurements were carried out at least three times for each flow rate. The error in the pressure readings was less than 0.5 %. A relationship between the flow and pressure drop was established using the pressure data for different flow rates. The energy dissipation rate per unit mass,  $\epsilon$  (W/kg), was calculated as:

$$\varepsilon = \frac{Q\Delta P}{\rho V} \quad (1)$$

where,  $Q$  is flow rate through the device ( $\text{m}^3/\text{s}$ ),  $\Delta P$  is the pressure drop across the device (Pa),  $\rho$  is the density of fluid passing through the device ( $\text{kg}/\text{m}^3$ ) and  $V$  is the volume of the device ( $\text{m}^3$ ). The micro-mixing performance at different rates of energy dissipation was investigated by varying the recirculation flow rate to cover a broad range of energy dissipation rates ( $\varepsilon = \sim 10^{-1}$ – $10^4$  W/kg).

## 2.2. Experimental procedure for characterising micro-mixing

The Villiermaux Dushman iodide-iodate parallel competitive reaction system is used for characterising micro-mixing [30,43]. Villiermaux Dushman reaction system comprises of two parallel competitive reactions R1 and R2. The first one being a neutralization reaction (instantaneous) and the second one being a redox reaction (fast – reaction time scale comparable to micro-mixing time).



In addition to these two main reactions, a third reaction R3 also needs to be considered. The iodine formed reacts with iodide to form triiodide which is a quasi-instantaneous equilibrium [30,43]:



These reactions are carried out in such a way that the acid ( $H^+$ ) is the limiting reactant. The reaction R1 is much faster than the reaction R2. Therefore, if micro-mixing is fast (compared to the characteristic time scale of the reaction R1, borate ions ( $H_2BO_3^-$ ) will rapidly consume  $H^+$  and there will be no opportunity for  $H^+$  to react with iodide ( $I^-$ ) and iodate ( $IO_3^-$ ) – that is the reaction R2 will not occur in such a case. If micro-mixing is not rapid, there will be opportunity for the reaction R2 to occur since a part of  $H^+$  which is not reacted with borate ions ( $H_2BO_3^-$ ) will be available. The yield of the product from the second reaction R2 ( $I_2$ ) is therefore used to quantify the micro-mixing efficiency of a mixer/reactor. Since the  $I_2$  formed via reaction R2 reacts with  $I^-$  and forms triiodide ( $I_3^-$ ), it is necessary to account for reaction R3 for appropriately calculating the yield of  $I_2$ . The kinetics of these reactions has been reported by many previous studies [28,30,42,43] and therefore not repeated here. For the sake of completeness, the details of previously reported kinetics are included in Section S1 of the Supplementary Information.

For carrying out these reactions, sulphuric acid ( $H_2SO_4$ ) (Fischer Scientific, 98 % concentrated) was chosen as the source of  $H^+$  ions. The buffer solution was prepared in a basic environment to avoid any premature triiodide formation [27]. The borate buffer was prepared using sodium hydroxide (Fischer Scientific, 98 % pure) and boric acid ( $H_3BO_3$ ) (Fischer Scientific, 99+% pure). Potassium iodide (KI) (Fischer Scientific, 99 % pure) and potassium iodate ( $KIO_3$ ) (Sigma Aldrich, >98 % pure) were added to this buffer solution, to match the required concentration. For all the chemicals, the % indicates wt.%. The different concentration sets were chosen from the literature and the nomenclature of the concentration sets has been retained as given by Commenge and Falk [30]. Villiermaux Dushman test reactions are independent of the reactant concentrations used [30,32,44]. The same has been verified with two different concentration sets (see Supplementary Information section S5) and concentration set 2B was selected for studying micro-mixing of the fluidic devices. The details of this concentration set 2B used in this study are given in Table 3.

The samples from the outlet, Fig. 1, were collected after four residence times of operation to ensure steady state. The collected samples were analysed for triiodide concentrations using a Shimadzu Spectrophotometer (UV-1800) equipped with high-precision quartz glass

**Table 3**  
Concentration set used in the study.

Component	Concentration set 2B (mol L <sup>-1</sup> )
$H^+$	0.03
$H_3BO_3$	0.045
$NaOH$	0.045
$KIO_3$	0.003
$KI$	0.016

cuvettes (Hellma Analytics 114-10-40) of 1 cm path length. Before analysing the samples, a calibration curve with the known concentrations of triiodide was obtained by measuring the absorbance at 353 nm [27,30,31,41] (see Supplementary Information section S2). The molar extinction coefficient ( $\epsilon_{353}$ ) was  $22,527 \text{ L mol}^{-1} \text{ cm}^{-1}$  as determined from the calibration curve. Guichardon et al. [27] earlier reported that the sample remains stable up to 30 min after acid injection. The samples were therefore analysed within 30 min of the experiment.

Furthermore, there has been a lot of discussion on the choice of acid in Villiermaux Dushman reactions. Sulphuric acid is commonly used acid as a source of  $H^+$  [27,40,43,44]. There are also published studies with monoprotic acids like perchloric and hydrochloric [32,44,52]. The use of perchloric acid poses problems of corrosion regardless of concentrations and it becomes unstable in cases of contact with hot surfaces and higher friction. This leads to the danger of an explosion [53]. Thus, due to safety concerns perchloric acid was not used in this work. As far as hydrochloric acid is considered, Guichardon et al. [54] reported formation of  $I_2Cl$  which would result in lower yield of triiodide ultimately underestimating the micro-mixing time. On the contrary, Schmitz [55] reported that the chloride ions act as catalysts for iodide oxidation leading to higher triiodide yield compared to other acids. Commenge and Falk [30] reported that there is no significant impact of acid (perchloric vs sulphuric) in Villiermaux Dushman reactions. Sulphuric acid was selected in this work to eliminate any ambiguity and ensure accuracy in the triiodide yield.

The pH of the buffer solution and final reaction mixture was measured offline using a pH meter (DFRobot's Gravity pH meter V2). Prior to using the pH probe, it was calibrated with known buffer solutions of pH = 4, pH = 7 and pH = 10. The pH of the buffer solution is a crucial parameter. At strongly basic pH, no iodine can form from iodide and iodate [53]. Furthermore, if the pH is far above the iodine dismutation pH  $\sim 7$ , the formed iodine will be thermodynamically unstable [27,53]. Thus, the working pH should be slightly above the iodine dismutation pH. Guichardon and Falk [27] reported that the pH of the buffer solution should range between 8.5 and 9.5. In this work, the pH of the borate buffer was  $9.47 \pm 0.05$  over different set of experiments conducted. The pH of the product in all the experiments was found to be around  $8.52 \pm 0.02$ . Thus, in this work, all the required conditions for pH for the Villiermaux Dushman reactions were satisfied.

It is essential to calculate the concentration of iodine from the measured triiodide concentration for calculating the extent of second reaction – quantified here in terms of the segregation index ( $X_S$ ) defined as:

$$X_S = \frac{Y}{Y_{ST}} \quad (2)$$

Where  $Y$  is the ratio of moles of acid consumed in the reaction R(2) to the moles of acid fed and  $Y_{ST}$  is the limiting value of  $Y$  [27] which are given as:

$$Y = \frac{2(q_1 + q_2)(C_{I_2} + C_{I_3^-})}{q_1 C_{H^+ o}} \quad (3)$$

$$Y_{ST} = \frac{6C_{IO_3^- o}}{6C_{IO_3^- o} + C_{H_2BO_3 o}} \quad (4)$$

For perfect mixing,  $X_S = 0$ . In the case of total segregation,  $X_S = 1$ . The relevant mass balances for iodine species and determination of iodine concentration from triiodide concentration has been explained in the [Supplementary Information](#) (Section S3). The experimental results of  $X_S$  were used to estimate micro-mixing time using the model discussed in [Section 3](#).

### 3. Computational model to estimate micro-mixing time

#### 3.1. Engulfment model for the loop configuration

As discussed in [Section 2.1](#), the experimental set-up includes an internal recirculation loop. The circulation within the loop (0.5 – 3 s) is orders of magnitude lower than the residence time (60 – 90 s). The characteristic reaction time scales of R1 ( $10^{-10}$  s) are much smaller than the circulation time. Considering the range of energy dissipation rates ( $10^{-1} - 10^4$  W/kg), it is expected that micro-mixing time scales (0.01 – 0.2 s) are also smaller than the circulation time. Therefore, it can be assumed that mixing is complete before one circulation time and the completely mixed streams which are depleted of the limiting reactant are circulated back after part of it exited via the outlet. The schematic of this physical picture is shown in [Fig. 2](#).

Ranade [2] has discussed appropriate reactor modelling approaches for different scenarios having different extents of micro-mixing and macro-mixing. It will be useful to estimate characteristic time scales for the considered case in this work as:

$$\text{Reaction time scale, } t_R = \frac{1}{k_1 C_0} = 10^{-10} \text{ s.}$$

Where  $k_1$  is a second order rate constant of reaction R(1) and  $C_0$  is a characteristic concentration of reactant.

$$\text{Macro-mixing, } t_{macro} = t_c = \frac{V}{Q_c} = 0.5 - 3 \text{ s.}$$

Where  $t_c$  is a circulation time,  $V$  is a reactor volume and  $Q_c$  is the net circulation flow rate.

$$\text{Micro-mixing time, } t_{micro} = 17.25 \sqrt{\frac{\nu}{\varepsilon}} = 0.01 - 0.2 \text{ s.}$$

Where  $\nu$  is kinematic viscosity and  $\varepsilon$  is energy dissipation rates.

$$\text{Process time scale or residence time, } \tau = \frac{V}{(q_1 + q_2)} = 60 - 90 \text{ s.}$$

It can be seen that for the case considered here, the reaction R(1) is very fast with characteristic time scale smaller than micro mixing time scales and the macro-mixing time scale is much smaller than the residence time of the reactor. In such cases, the performance of a reactive flow process is controlled only by the micro-mixing. Several micro-mixing models have been developed to simulate such reactive flow processes. Some of the widely used models are:

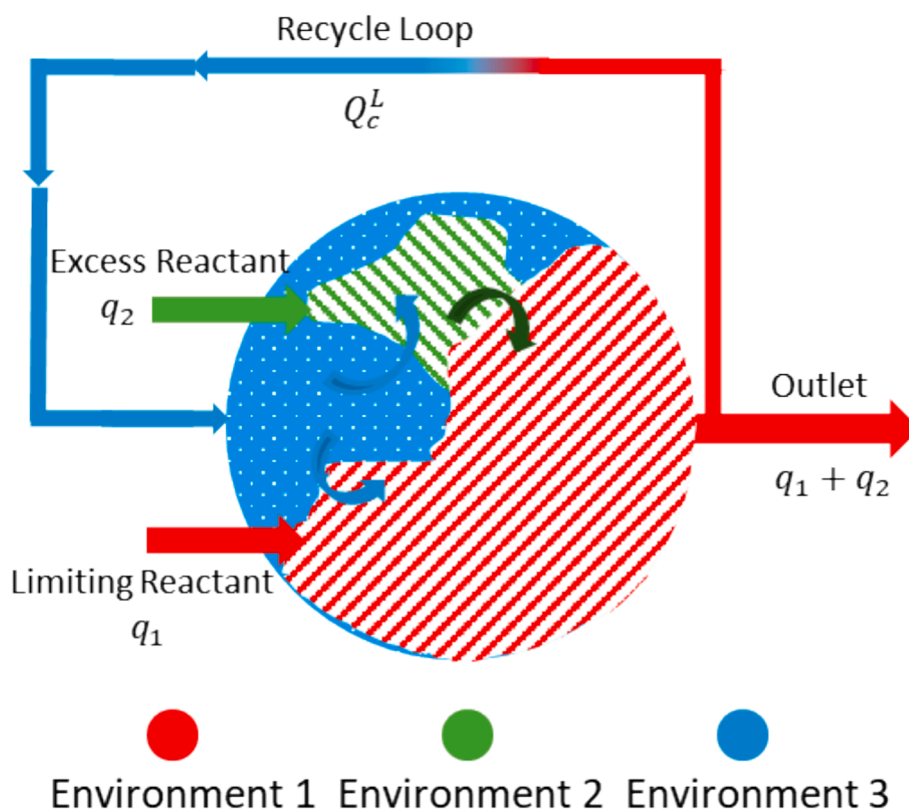
- ‘Engulfment Deformation Diffusion (EDD)’ model of Baldyga and Bourne [37]
- ‘Interaction by Exchange with the Mean (IEM)’ model of David and Villermaux [36,56]
- ‘Engulfment (E)’ model of Baldyga and Bourne [35]

In this work, we used the engulfment model and extended it so as to make it applicable to the experimental set-up used in this work. Instead of the classical two-environment model of Baldyga and Bourne [35], we used three-environments represented in the schematic shown in [Fig. 2](#). The net internal circulation flow rate is:

$$Q_c = q_1 + q_2 + Q_c^L \quad (5)$$

Where  $Q_c^L$  is the flow rate through a recycle loop.

The Environment 1 which is a reacting zone corresponds to a stream carrying a limiting reactant. The volume of Environment 1 will grow by engulfing Environment 2 (second feed stream) as well as Environment 3 (recirculated stream). The volume of Environment 3 will reduce with time. The volume of Environment 2 may increase initially via engulfment of Environment 3 and will eventually reduce because of engulfment by Environment 1. The growth of the volumes of these



**Fig. 2.** Schematic of reactor in loop configuration [Environment 1 contains the limiting reactant and is the only environment where reactions take place. Environment 1 engulfs Environments 2 (corresponding to feed stream 2 containing other reactants) and Environment 3 (corresponding to recirculation stream)].

environments and species balances may be written as:

$$\frac{dV_1}{dt} = E \frac{V_1 V_3}{V} + E \frac{V_1 V_2}{V} \quad (6)$$

$$\frac{dV_2}{dt} = -E \frac{V_1 V_2}{V} + E \frac{V_2 V_3}{V} \quad (7)$$

$$\frac{dV_3}{dt} = -E \frac{V_1 V_3}{V} - E \frac{V_2 V_3}{V} \quad (8)$$

$$\frac{d(V_1 + V_2 + V_3)}{dt} = 0 \quad (9)$$

Where  $E$  is engulfment rate (which is a reciprocal of micro-mixing time scale) and  $t$  is time.

The species balance for the segregated environments may be written as:

$$\frac{dC_{k1}}{dt} = E \frac{V_3}{V} (C_{k3} - C_{k1}) + E \frac{V_2}{V} (C_{k2} - C_{k1}) + R_{k1} \quad (10)$$

$$\frac{dC_{k2}}{dt} = E \frac{V_3}{V} (C_{k3} - C_{k2}) \quad (11)$$

$$\frac{dC_{k3}}{dt} = 0 \quad (12)$$

$C_{kj}$  is concentration of species  $k$  in environment  $j$ . It is assumed that at the end of one circulation time, all three environments are mixed since the characteristic micro-mixing time scale is smaller than the circulation time scale. The concentration of species  $k$  in this mixed stream will be same as the concentration of species  $k$  in the outlet ( $C_{ko}$ ) and is calculated as:

$$C_{ko} = \frac{V_1 C_{k1} + V_2 C_{k2} + (V - V_1 - V_2) C_{k3}}{V} \quad (13)$$

This outlet stream is recirculated back to the reactor where the incoming streams encounter species with these concentrations as the bulk zone. Initial conditions for these ODEs may be written as:

At  $t = 0$  :

$$V_1 = t_f q_1, V_2 = t_f q_2, V_3 = V - V_1 - V_2$$

Where  $t_f$  is a characteristic feed time which may be assumed to be a small fraction of circulation time,  $t_c$ . In this work,  $t_f$  was set to 0.01 times  $t_c$ .

$$C_{k1} = C_{k1i}, C_{k2} = C_{k2i}, C_{k3} = C_{ko}$$

Where subscript  $i$  indicates inlet stream.

These transient ODEs are solved till all the limiting reactant is consumed or  $V_1 = V$  or  $t = t_c$ , whichever is earlier.

The three-environment engulfment model described in this section is a generalized model applicable to any reaction scheme and reactor operated in a loop configuration. Villiermaux Dushman reactions contain six components namely  $H^+$ ,  $H_2BO_3^-$ ,  $H_3BO_3$ ,  $I^-$ ,  $IO_3^-$  and  $I_2$ . The first two reactions (R1 and R2) were simulated using the model. The concentration of  $I_3^-$  was calculated using the equilibrium constant which was then used to find  $X_S$ . The micro-mixing time,  $t_{micro}$  was an input to the model and  $X_S$  was calculated once all the concentrations were obtained from the model. Large number of simulations covering the broad range of characteristic micro-mixing time were carried out. The simulated results exhibit the following linear relationship between  $X_S$  and  $t_{micro}$  (s) over the considered range in this work as (see Fig. S3a of Supplementary Information):

$$t_{micro} = 3.4X_S \quad (14)$$

The model developed here exhibits non-linear relationship between  $X_S$  and  $t_{micro}$  at higher values of  $X_S$ . A review of previous studies reveals

broadly two groups: one group reports the multiplier of  $X_S$  appearing in Equation (14) as  $\sim 0.1$  while the other group reports it as  $\sim 3$ . Gobert et al. [41] have reported a slope of 0.08 for the concentration set 2B. Chen et al. [47] reported  $t_{micro} = 0.072X_S^{1.08}$  (for a different concentration set with annular rotating flow mixer – refer to Table 1). The micro-mixing times reported by Gobert et al. and Chen et al. are therefore quite small (in the range of 0.1–1 ms) compared to those reported by others. El-Shazly et al. [44] have reported the slope of  $t_m$  vs  $X_S$  for concentration set 2B as 4. Guo et al. [43] reported a slope of 2.55 for their concentration set. The micro-mixing times reported by this second group of investigators are therefore in the range of 10 to 100 ms. In the present work, the linear fit was adequate for the considered range and therefore Equation (14) was used for relating experimentally observed  $X_S$  with  $t_{micro}$ . Falk and Commenge [57] reported that with Villiermaux Dushman reactions and any method of mixing time determination, the accuracy cannot be better than  $\pm 30\%$ . Equation (14) was used to estimate micro-mixing time scales for three devices for different operating conditions. The  $\pm 30\%$  variation of the parameter in Equation (14) encompass the range from 2.4 to 4.4 which covers the parameters reported in previous studies. The micro-mixing times estimated using Equation (14) are discussed in the following section.

#### 4. Results and discussion

Micro-mixing performances of fluidic devices (micro-mixing times) are usually evaluated with reference to mean energy dissipation rate,  $\epsilon$  [34,35]. The pressure drops as a function of flow rate through the fluidic devices was therefore characterised to enable the calculation of mean energy dissipation rates using Equation (1). The measured pressure drop values were then reported as a function of Reynolds number and are shown in Fig. 3a. Characteristic length scales ( $d_c$ ) and characteristic area ( $A_c$ ) were used to convert flow rates to Reynolds number as:

$$Re = \frac{d_c \rho Q}{\mu A_c} \quad (15)$$

Where  $\mu$  is the viscosity,  $\rho$  is the density of the fluid and  $Q$  is the volumetric flow rate.

The pressure drop and mean energy dissipation rate were correlated with the Reynolds number as:

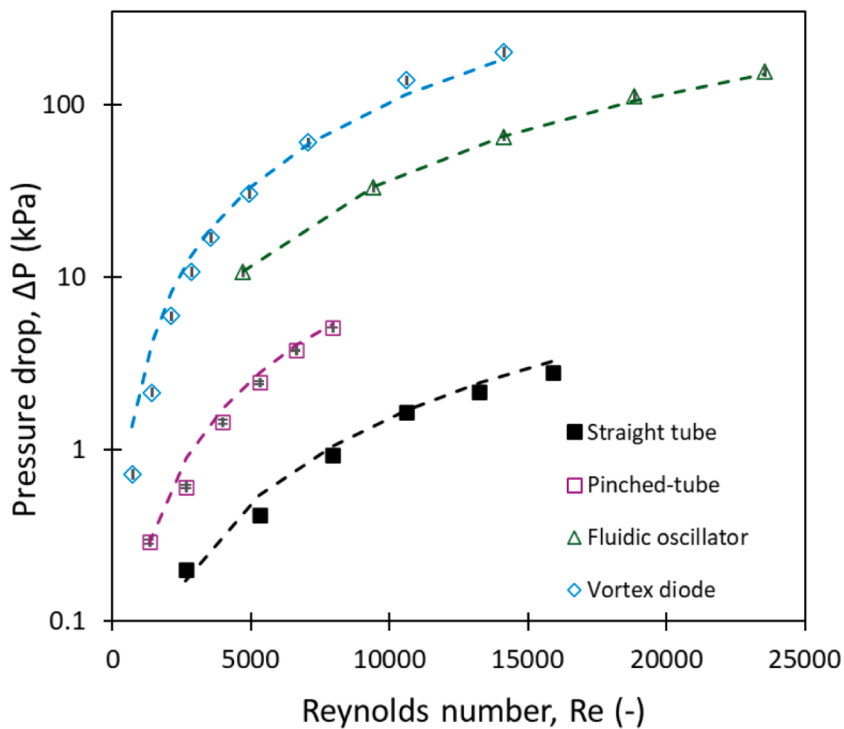
$$\Delta P = \Delta P_{Re=5000} \left( \frac{Re}{5000} \right)^b \quad (16)$$

$$\epsilon = \epsilon_{Re=5000} \left( \frac{Re}{5000} \right)^{b+1} \quad (17)$$

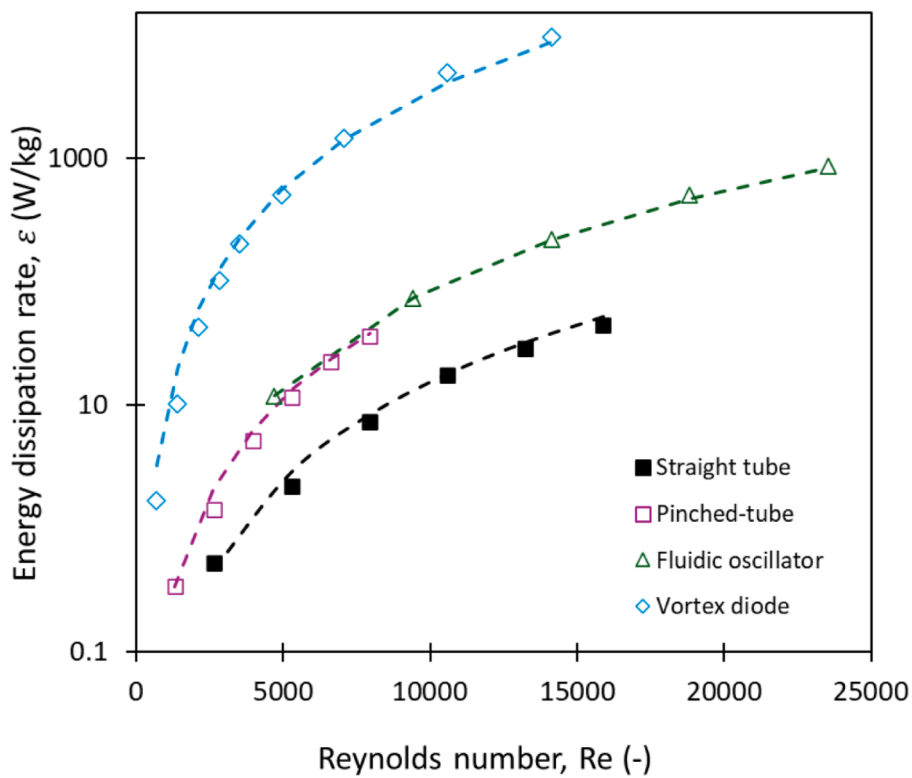
where,  $\Delta P_{Re=5000}$  and  $\epsilon_{Re=5000}$  are the values of pressure drop and rate of energy dissipation corresponding to  $Re = 5000$  and  $b$  is a fitted parameter. The value of  $b$  was found to be 1.64 for all the devices. The rate of energy dissipation as a function of  $Re$  is shown in Fig. 3b. The rate of energy dissipation was calculated using Equation (1). It can be seen from Fig. 3b that the devices studied in this work cover a wide range of  $\epsilon$  – lowest being exhibited by the straight tube and highest being exhibited by the vortex diode.

After characterising energy dissipation rates of these devices, the Villiermaux Dushman reactions were carried out and concentrations of the products were used to calculate the segregation index,  $X_S$ . The segregation index,  $X_S$  calculated based on the measured values of triiodide as a function of  $Re$  for the devices considered in this work is shown in Fig. 4.

It can be seen that for three fluidic devices – straight tube, pinched-tube and fluidic oscillator, an increase in  $Re$  leads to reduction in segregation index. This reduction in  $X_S$  indicates improved mixing with an increase in  $Re$  (or in mean energy dissipation rates). It can be seen that pinched-tube and fluidic oscillator lead to lower  $X_S$  values



(a)



(b)

Fig. 3. Flow characterisation of fluidic devices considered in this work with (a) pressure drop as a function of Reynolds number (b) mean energy dissipation rates as function of Reynolds number for all fluidic devices. Symbols denote experimental data. Dotted lines indicate predictions using Equation (16) and (17).

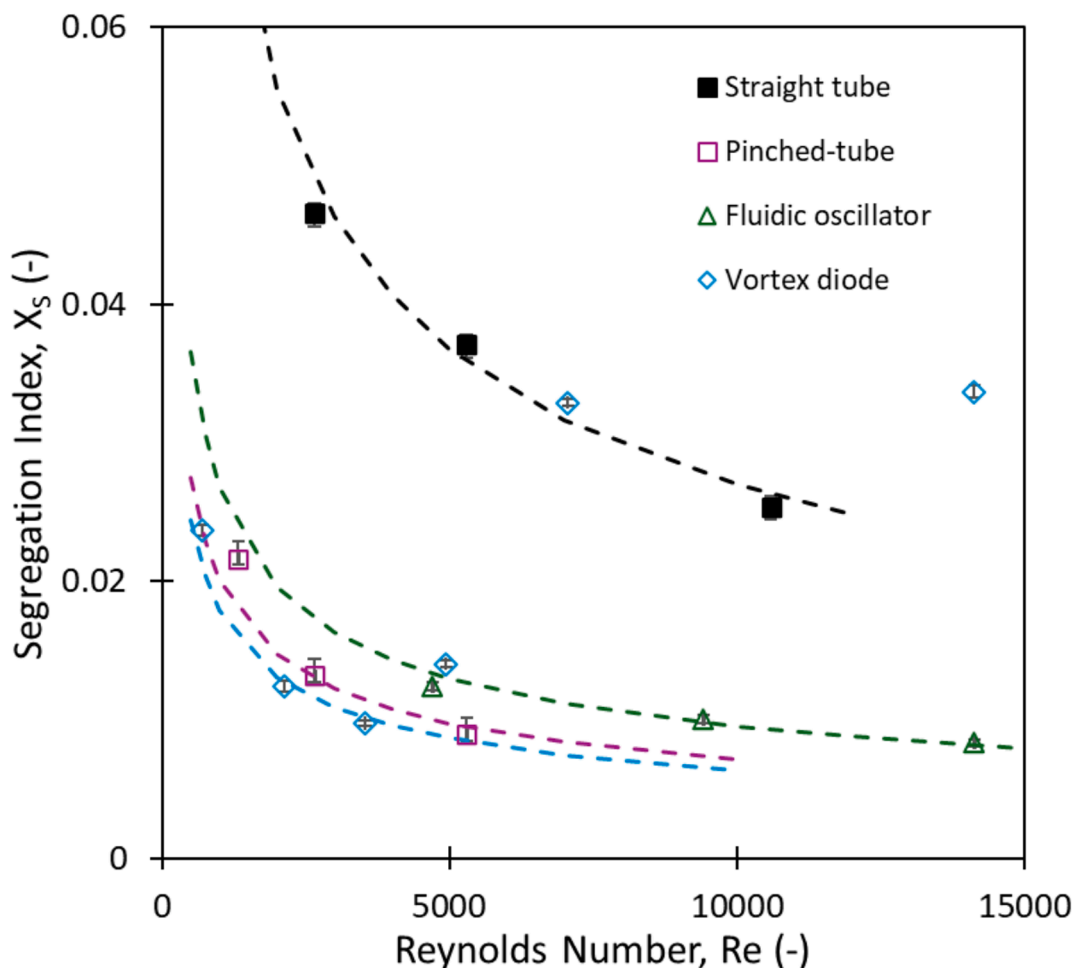


Fig. 4. Experimentally measured segregation index as a function of Reynolds number of the fluidic devices used in this work. Symbols denote experimental data. Dashed lines show power-law trend lines (Equation (18)).

compared to the straight tube. The dashed lines shown in Fig. 4 indicate power law behaviour as per the following equation:

$$X_s = pRe^{-0.45} \quad (18)$$

The value of parameter  $p$  was found to be 1.7 for straight tube, 0.45 for pinched-tube, 0.4 for vortex diode (before the inception of cavitation) and 0.60 for fluidic oscillator. For the cavitating device, the measured segregation index was found to increase with an increase in  $Re$  once the cavitation inception occurs (for  $Re > 4000$ ). The cavitation inception occurs at around  $Re \sim 4000$ . Cavitation leads to the formation of hydroxyl radicals [26,39,58] which interfere with the Villermaux Dushman reactions and cause an increase in  $X_s$  with increase in extent of cavitation [59,60]. Hence, additional control experiments were conducted in the absence of  $[H_2BO_3^-]$ . Initial experiments were carried out to examine the potential decomposition of KI due to hydrodynamic cavitation. A 0.016 M KI solution was passed through the vortex diode. No triiodide peak was detected with recirculation flow rates of 0.3 – 2 L  $min^{-1}$ . In the Villermaux Dushman reactions, acid is present in the system which may influence the oxidising performance of hydrodynamic cavitation. Two sets of experiments were therefore carried out at two different acid concentrations in the absence of  $[H_2BO_3^-]$ . In the first case, the acid concentration was kept the same as in the Villermaux Dushman reactions ( $[H^+] = 0.03 \text{ mol L}^{-1}$ ) and in the second case, 200 times lower acid concentration was used ( $[H^+] = 0.00015 \text{ mol L}^{-1}$ ). The increase in concentration of triiodide with reference to that measured just before cavitation inception with respect to Reynolds number for these cases is shown in Fig. 5.

It can be seen that at high acid concentration, hydrodynamic cavitation leads to triiodide concentration even in the absence of  $[H_2BO_3^-]$ . The conventional method of measuring micromixing time using the Villermaux Dushman reaction therefore is not directly applicable to cases where cavitation occurs. Micromixing time of cavitating devices may therefore be estimated before the inception of cavitation and may be extrapolated for cavitating conditions.

The micro-mixing time in the fluidic devices under consideration as a function of  $\varepsilon$  can be obtained as:

$$t_{micro} = t_{micro\varepsilon=1} e^{-\frac{0.45}{b+1}\varepsilon} \quad (19)$$

where,  $t_{micro\varepsilon=1}$  is the micro-mixing time corresponding to  $\varepsilon = 1 \text{ W/kg}$ . Using the known value of  $b$ , Equation (19) can be written as:

$$t_{micro} = t_{micro\varepsilon=1} \varepsilon^{-0.17} \quad (20)$$

The values of  $t_{micro\varepsilon=1}$  for straight tube, pinched-tube, fluidic oscillator and vortex diode are 146 ms, 50 ms, 66 ms and 85 ms respectively. The micro-mixing time is usually reported as a function of rate of energy dissipation,  $\varepsilon$ . The micro-mixing time of all the considered devices as a function of energy dissipation rate is shown in Fig. 6. All the devices exhibit micro-mixing time proportional to  $\varepsilon^{-0.17}$ . It can be seen that for a given rate of energy dissipation, the pinched tube outperforms the vortex diode and fluidic oscillator, which show almost the same performance. For the case of vortex diode, the segregation index was found to increase with energy dissipation rate after the inception of cavitation – which indicates a higher micro-mixing time scale. However, this

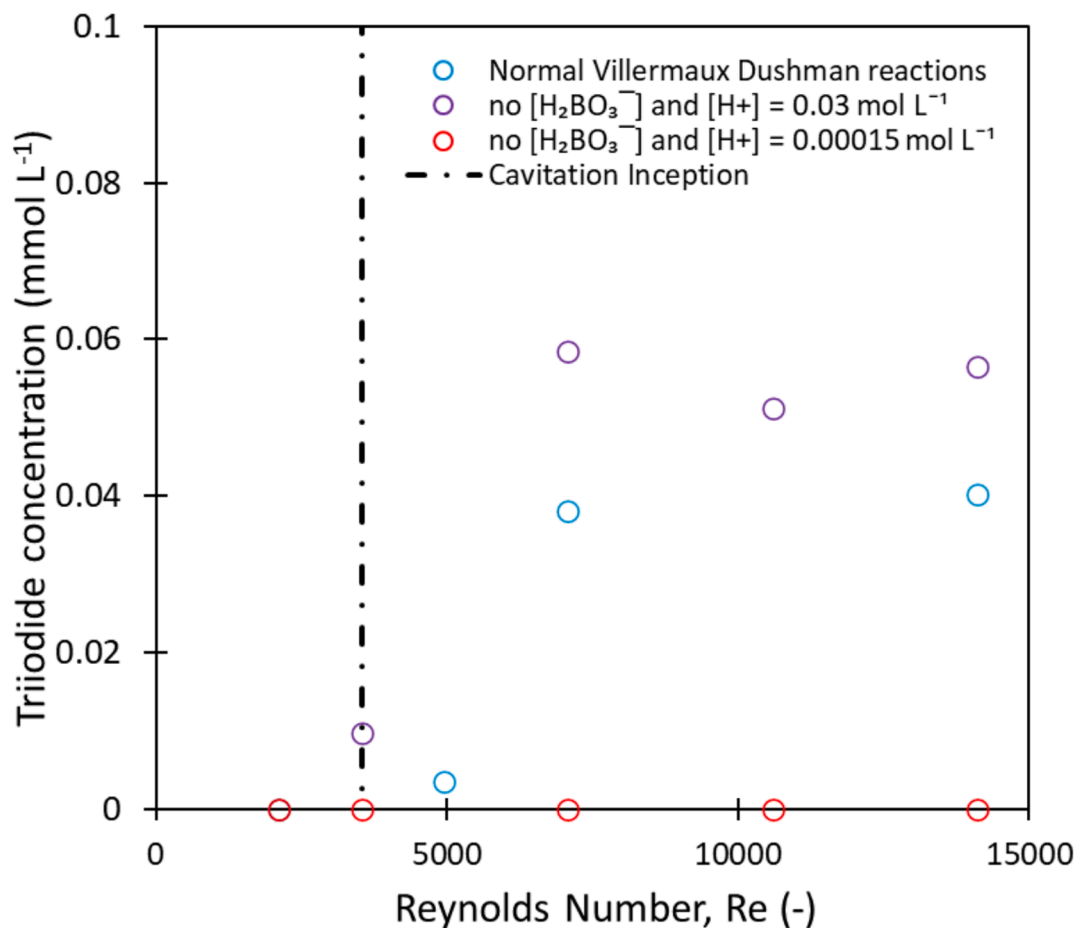


Fig. 5. Measured triiodide concentration beyond cavitation inception in vortex diode for three cases – normal Villermaux Dushman reactions and in absence of  $[H_2BO_3^-]$  with different acid concentrations.

increase is because of interference of cavitation with Villermaux Dushman reactions. If the data points are extrapolated from the results obtained prior to inception of cavitation (along the blue dashed line in Fig. 6), the vortex diode would exhibit the lowest micro-mixing time among the studied devices since it offers much higher energy dissipation rates. When the absolute values of micro-mixing times are compared, the straight tube has the largest micro-mixing time among the studied devices. It exhibits micro-mixing time of about 100 ms at  $\varepsilon$  of about 10 W/kg. For the same energy dissipation rate, the pinched-tube exhibits the lowest micro-mixing time of  $\sim 30$  ms while the fluidic oscillator and vortex diode exhibit about 40 ms and 50 ms respectively. For obtaining micro-mixing time of 30 ms, the energy dissipation rate needs to be increased to nearly 80 W/kg for the fluidic oscillator and 200 W/kg for the vortex diode.

Once clear trends of micro-mixing time as a function of rate of energy dissipation were obtained for the devices used in this study, the micro-mixing times obtained for the three devices were compared with those reported in the published studies in Fig. 7. The solid lines denote power law relationship similar to Equation (20) with the  $t_{micro}$  proportional to  $\varepsilon^{-0.15}$ ,  $\varepsilon^{-0.30}$ ,  $\varepsilon^{-0.45}$ ,  $\varepsilon^{-0.60}$  for the pink, green, orange and blue lines respectively. Commenge and Falk [30] and Baldyga and Bourne [61] reported that the micromixing time is proportional to  $\varepsilon^{-0.45}$  and  $\varepsilon^{-0.5}$  respectively. It is evident from Fig. 7 that the micro-mixing time of devices considered in this work and many other devices/mixers from published studies falls in the range proportional to  $\varepsilon^{-0.15}$  and  $\varepsilon^{-0.3}$ . Chen et al. [47] investigated micro-mixing characteristics of a rotating annular flow mixer using Villermaux Dushman reactions and obtained a trend, where beyond a certain  $\varepsilon$  (1500 W/kg), the micro-mixing time

increased with an increase in  $\varepsilon$ . They attribute the increase in the micro-mixing time to the 'entrainment regime' where the energy utilization is low. The multichannel heat exchanger designs reported by Guo et al. [43] (M1 and M2) show behaviour similar to the devices in the present study. The micro-mixing time obtained for M1 and M2 was found to be proportional to  $\varepsilon^{-0.2}$ . The impinging jet mixer (IJM) shows proportionality as  $\varepsilon^{-0.45}$ . The Syrris micromixer shows a flat trend across the range of energy dissipation rates. The MARB mixer shows higher slope than the standard correlations and the authors have attributed the same to high energy utilization of the mixer. The micro-mixing time for IJSDR shows dependence as  $\varepsilon^{-0.4}$ . Abiev et al. [62] reported micromixing time of a swirling flow micromixer having two tangential inlets to proportional to  $\varepsilon^{-0.21}$  (not shown in Fig. 7). The reasons for these observed differences in the dependence of micro-mixing time with  $\varepsilon$  may be because of specific flow structures and the way shear and turbulence are harnessed for accelerating mixing. Detailed computational fluid dynamics models developed for the pinchedtube [12], fluidic oscillators [63,64] and vortex diode [65] need to be extended further for simulating micro-mixing in these devices for developing better understanding of micromixing in these devices. The presented data will be useful for validating such models.

The pinched-tube, fluidic oscillator and vortex-based cavitation device investigated in this work offer a wide range of energy dissipation rates and therefore micro-mixing times from 30 ms onwards. The presented results will be useful for appropriate selection of devices and their operating parameters for desired applications like reactive precipitation, nanoparticles synthesis, anti-solvent crystallization, etc. The key quality attributes of the products of such processes are strongly influenced by

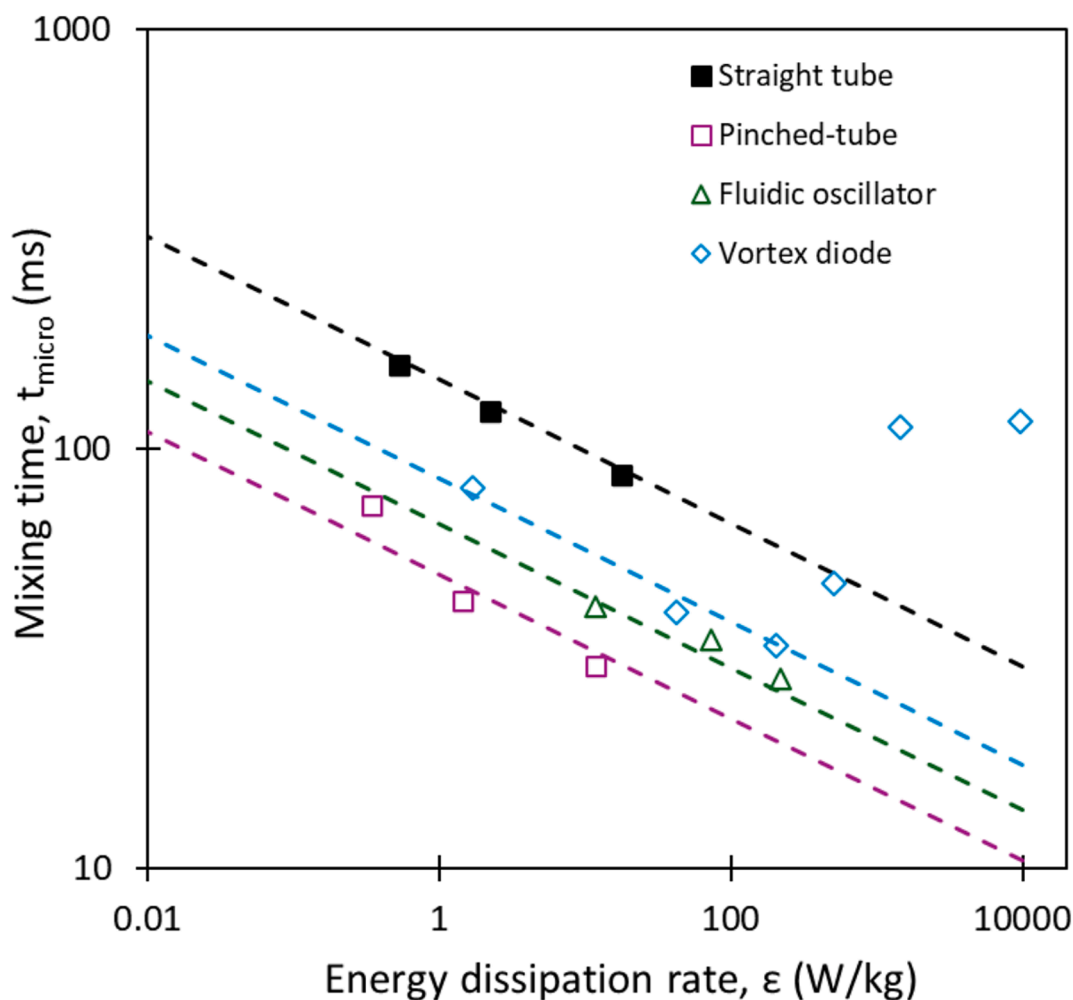


Fig. 6. Variation of micro-mixing time with mean energy dissipation rates for the fluidic devices under consideration. Symbols denote experimental results. Lines denote power law relationships given in Equation (20).

micro-mixing times. For example, results of Song et al. [66] indicate that there is a direct link between the micro-mixing time and the size of lipid-polymer hybrid nanoparticles produced. Similar results were reported by Gradl and Peukert [67] for barium sulphate nanoparticles synthesized by reactive precipitation. It is therefore essential to first identify the desired micro-mixing time and then select an appropriate fluidic device and corresponding operating parameters to achieve the desired micro-mixing time. The work presented in this manuscript provides a methodology to estimate micro-mixing time using Equation (19). Once the desired micro-mixing time is identified, Equations (16), (17) and (19) may be used to identify appropriate Reynolds number and hence the recirculation flow rate through the loop. Depending on the range of desired micro-mixing time, Fig. 6 may be used to select an appropriate fluidic device. As a part of future work, we are working on the synthesis of lipid nanoparticles via antisolvent precipitation using these fluidic devices. The objective is to tailor the particle size and polydispersity of the particles using these fluidic devices and controlling micro-mixing times and other relevant process parameters.

## 5. Conclusions

In this work, we have investigated micro-mixing characteristics of pinched-tube, fluidic oscillator and vortex-based cavitation device over a wide range of operating parameters and energy dissipation rates ( $10^{-1}$  to  $10^4$  W/kg). A three-environment engulfment model was developed and used to simulate micro-mixing in these three devices operated in a

loop configuration. The key conclusions of this work are:

- Pressure drops across the three fluidic devices studied in this work were found to be proportional to Reynolds number to the power 1.64 (Equation (16))
- The developed three-environment engulfment model led to linear relationship between the segregation index,  $X_S$  and micromixing time,  $t_{micro}$  over the operating range considered in this work (Equation (14)).
- The estimated micro-mixing time was proportional to  $\epsilon^{-0.17}$  for all the devices (Equation (20))
- For  $\epsilon$  of 10 W/kg, the pinched-tube exhibited the lowest micro-mixing time of about 30 ms. The fluidic oscillator requires  $\sim 80$  W/kg and the vortex diode requires  $\sim 200$  W/kg for realising micro-mixing time of about 30 ms.
- The measurements of micro-mixing times for the vortex-based cavitation device was hampered by the inception of cavitation. The segregation index was found to increase with further increase in energy dissipation rates beyond cavitation inception. Villermaux Dushman reactions are therefore not suitable for characterising micro-mixing in cavitating devices.

The mixing results presented in this work provide a basis for selection of appropriate device and associated operating parameters for carrying out processes that are kinetically fast and mixing controlled.

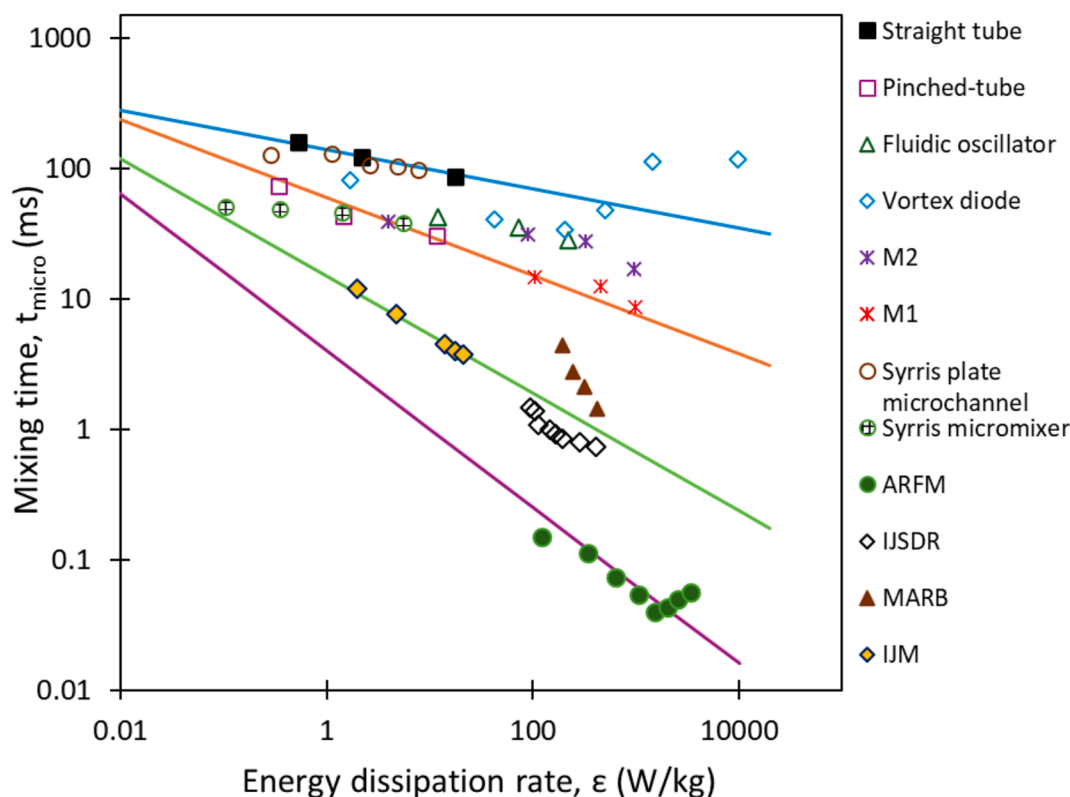


Fig. 7. Variation of micro-mixing time with mean energy dissipation rates – present work and published studies. (For abbreviations of mixers/devices refer to Table 1).

#### CRedit authorship contribution statement

**Amol N. Joshi:** Data curation, Formal analysis, Investigation, Methodology, Validation, Writing – original draft. **Amol V. Ganjare:** Investigation, Data curation. **Sarah Hudson:** Writing – review & editing, Supervision, Project administration, Methodology. **Vivek V. Ranade:** Writing – review & editing, Supervision, Project administration, Methodology, Investigation, Funding acquisition, Conceptualization.

#### Declaration of competing interest

The authors declare that they have no known competing financial interests or personal relationships that could have appeared to influence the work reported in this paper.

#### Acknowledgements

The authors greatly acknowledge the financial support by the School of Chemical Sciences and Chemical Engineering, University of Limerick and UL Foundation (Project ID 57683). One of the authors (AG) would like to acknowledge PMTC (<https://pmtc.ie/>) and SSPC (<https://sspc.ie/>) for partially supporting the work. The authors would like to thank Dr. Chinmay Shukla for engaging in technical discussions.

#### Appendix A. Supplementary data

Supplementary data to this article can be found online at <https://doi.org/10.1016/j.cej.2025.163657>.

#### Data availability

Data will be made available on request.

#### References

- [1] J.R. Bourne, J. Baldyga, The effect of micromixing on parallel reactions, *Chem. Eng. Sci.* 45 (1990) 907–916, [https://doi.org/10.1016/0009-2509\(90\)85013-4](https://doi.org/10.1016/0009-2509(90)85013-4).
- [2] V.V. Ranade, *Computational Flow Modeling for Chemical Reactor Engineering*, Vol. 5, Academic Press, 2002.
- [3] R.S. Brodkey, *Turbulence in Mixing Operations: Theory and Application to Mixing and Reaction*, Academic Press, 1975.
- [4] J. Baldyga, R. Pohorecki, Turbulent micromixing in chemical reactors - a review, *Chem. Eng. J.* 58 (1995) 183–195.
- [5] A.K. Sahu, P. Kumar, A.W. Patwardhan, J.B. Joshi, CFD modelling and mixing in stirred tanks, *Chem. Eng. Sci.* 54 (1999) 2285–2293, [https://doi.org/10.1016/S0009-2509\(98\)00334-0](https://doi.org/10.1016/S0009-2509(98)00334-0).
- [6] J.R. Bourne, J. Lenzner, S. Petrozzi, Micromixing in static mixers: an experimental study, *Ind. Eng. Chem. Res.* 31 (1992) 1216–1222, <https://doi.org/10.1021/ie00004a037>.
- [7] M. Mridha, K.D.P. Nigam, Coiled flow inverter as an inline mixer, *Chem. Eng. Sci.* 63 (2008) 1724–1732, <https://doi.org/10.1016/j.ces.2007.10.028>.
- [8] J.P. Valdés, L. Kahouadji, O.K. Matar, Current advances in liquid–liquid mixing in static mixers: a review, *Chem. Eng. Res. Des.* 177 (2022) 694–731, <https://doi.org/10.1016/j.cherd.2021.11.016>.
- [9] C.M. Khalde, V. Ramanan, J.S. Sangwai, V.V. Ranade, Passive mixer cum reactor using threaded inserts: investigations of flow, mixing, and heat transfer characteristics, *Ind. Eng. Chem. Res.* 59 (2020) 3943–3961, <https://doi.org/10.1021/acs.iecr.9b04606>.
- [10] V.M. Barabash, R.S. Abiev, N.N. Kulov, Theory and practice of mixing: a review, *Theor. Found. Chem. Eng.* 52 (2018) 473–487, <https://doi.org/10.1134/S004057951804036X>.
- [11] K.D.P. Nigam, V.V. Ranade, I&EC research special issue on fluidic devices without moving parts, *Ind. Eng. Chem. Res.* 59 (2020) 3633–3635, <https://doi.org/10.1021/acs.iecr.0c00710>.
- [12] N.S. Hasabnis, K.A. Totlani, V.V. Ranade, Heat transfer and mixing in flow through pinched pipe, *Can. J. Chem. Eng.* 93 (2015) 1860–1868, <https://doi.org/10.1002/cjce.22275>.
- [13] Y. Yu, P.K.J. Robertson, V.V. Ranade, Continuous antisolvent crystallization using fluidic devices: fluidic oscillator, helical coil, and coiled flow inverter, *Ind. Eng. Chem. Res.* 61 (2022) 15000–15013, <https://doi.org/10.1021/acs.iecr.2c02504>.
- [14] M.K. Sharma, S.B. Potdar, A.A. Kulkarni, Pinched tube flow reactor: Hydrodynamics and suitability for exothermic multiphase reactions, *AIChE J.* 63 (2017) 358–365, <https://doi.org/10.1002/aic.15498>.
- [15] S. Asano, T. Maki, S. Inoue, S. Sogo, M. Furuta, S. Watanabe, Y. Muranaka, S. Kudo, J. Hayashi, K. Mae, Incorporative mixing in microreactors: Influence on reactions

- and importance of inlet designation, *Chem. Eng. J.* 451 (2023), <https://doi.org/10.1016/j.cej.2022.138942>.
- [16] A.V. Pandit, V.V. Ranade, Fluidic oscillator as a continuous crystallizer: feasibility evaluation, *Ind. Eng. Chem. Res.* 59 (2020) 3996–4006, <https://doi.org/10.1021/acs.iecr.9b04637>.
- [17] A.A. Kulkarni, V.V. Ranade, R. Rajeev, S.B. Koganti, Pressure drop across vortex diodes: experiments and design guidelines, *Chem. Eng. Sci.* 64 (2009) 1285–1292, <https://doi.org/10.1016/j.ces.2008.10.060>.
- [18] A. Hengelbrock, A. Schmidt, J. Strube, Formulation of nucleic acids by encapsulation in lipid nanoparticles for continuous production of mRNA, *Processes* 11 (2023) 1718, <https://doi.org/10.3390/pr11061718>.
- [19] K. Huanbutta, K. Suwanpitak, N. Weeranoppanant, P. Sriamornsak, K. Garg, S. Sharma, I. Singh, T. Sangnim, Continuous flow synthesis: a promising platform for the future of nanoparticle-based drug delivery, *J. Drug Deliv. Sci. Technol.* 91 (2024), <https://doi.org/10.1016/j.jddst.2023.105265>.
- [20] C.F. Rodríguez, V. Andrade-Pérez, M.C. Vargas, A. Mantilla-Orozco, J.F. Osma, L. H. Reyes, J.C. Cruz, Breaking the clean room barrier: exploring low-cost alternatives for microfluidic devices, *Front. Bioeng. Biotechnol.* 11 (2023), <https://doi.org/10.3389/fbioe.2023.1176557>.
- [21] K. Madane, V. Ranade, Jet oscillations and mixing in fluidic oscillators: influence of geometric configuration and scale, *Ind. Eng. Chem. Res.* (2023), <https://doi.org/10.1021/acs.iecr.3c02077>.
- [22] H.M. Xia, Y.P. Seah, Y.C. Liu, W. Wang, A.G.G. Toh, Z.P. Wang, Anti-solvent precipitation of solid lipid nanoparticles using a microfluidic oscillator mixer, *Microfluid. Nanofluidics* 19 (2015) 283–290, <https://doi.org/10.1007/s10404-014-1517-5>.
- [23] V.P. Sarvothaman, S.R. Kulkarni, J. Subburaj, S.L. Hariharan, V.K. Velisoju, P. Castano, P. Guida, D.M. Prabhudharwadkar, W.L. Roberts, Evaluating performance of vortex-diode based hydrodynamic cavitation device scale and pressure drop using coumarin dosimetry, *Chem. Eng. J.* 481 (2024), <https://doi.org/10.1016/j.cej.2024.148593>.
- [24] A.H. Thaker, P. Boreham, K.L. Kourousis, V.V. Ranade, Liquid-liquid emulsion produced by 3D-printed vortex-based hydrodynamic cavitation device, *Chem. Eng. Technol.* 46 (2023) 1970–1976, <https://doi.org/10.1002/ceat.202300061>.
- [25] P.B. Patil, P. Thanekar, V.M. Bhandari, Intensified hydrodynamic cavitation using vortex flow based cavitating device for degradation of ciprofloxacin, *Chem. Eng. Res. Des.* 187 (2022) 623–632, <https://doi.org/10.1016/j.cherd.2022.09.027>.
- [26] H. Zheng, Y. Zheng, J. Zhu, Recent developments in hydrodynamic cavitation reactors: cavitation mechanism, reactor design, and applications, *Engineering* 19 (2022) 180–198, <https://doi.org/10.1016/j.eng.2022.04.027>.
- [27] P. Guichardon, L. Falk, Characterisation of micromixing efficiency by the iodide-iodate reaction system. Part I: experimental procedure, *Chem. Eng. Sci.* 55 (2000) 4233–4243, [https://doi.org/10.1016/S0009-2509\(00\)00068-3](https://doi.org/10.1016/S0009-2509(00)00068-3).
- [28] J.R. Bourne, Comments on the iodide/iodate method for characterising micromixing, *Chem. Eng. J.* 140 (2008) 638–641, <https://doi.org/10.1016/j.cej.2008.01.031>.
- [29] K. Krupa, M.I. Nunes, R.J. Santos, J.R. Bourne, Characterization of micromixing in T-jet mixers, *Chem. Eng. Sci.* 111 (2014) 48–55, <https://doi.org/10.1016/j.ces.2014.02.018>.
- [30] J.M. Commenge, L. Falk, Villermaux-Dushman protocol for experimental characterization of micromixers, *Chem. Eng. Process.* 50 (2011) 979–990, <https://doi.org/10.1016/j.cep.2011.06.006>.
- [31] J. Pinot, J.M. Commenge, J.F. Portha, L. Falk, New protocol of the Villermaux-Dushman reaction system to characterize micromixing effect in viscous media, *Chem. Eng. Sci.* 118 (2014) 94–101, <https://doi.org/10.1016/j.ces.2014.07.010>.
- [32] T. Frey, F. Kexel, M. Grabellus, X.M. Le, M. Hoffmann, F. Herbstreit, M. Grünewald, M. Schlüter, Local analysis of micro mixing for the Villermaux-Dushman protocol by using the imaging UV-Vis spectroscopy, *Chem. Eng. Res. Des.* 205 (2024) 822–829, <https://doi.org/10.1016/j.cherd.2024.04.049>.
- [33] J. Villermaux, Macro and Micromixing Phenomena in Chemical Reactors, in: *Chemical Reactor Design and Technology*, Springer, 110 (1986)191–244, doi: 10.1007/978-94-009-4400-8\_6.
- [34] V.V. Ranade, J.R. Bourne, Reactive mixing in agitated tanks, *Chem. Eng. Commun.* 99 (1991) 33–53, <https://doi.org/10.1080/00986449108911577>.
- [35] J. Baldyga, J.R. Bourne, Simplification of Micromixing Calculations. I. Derivation and Application of New Model, 42 (1989) 83–92. doi: 10.1016/0300-9467(89)85002-6.
- [36] J. Villermaux, C. Devillon, Representation de la Coalescence et de la Redispersion des Domaines de Segregation dans un Fluides Par un Modele d'interaction Phénoménologique, in: *2nd International Symposium Chem. React. Eng.* 1972.
- [37] J. Baldyga, J.R. Bourne, A fluid mechanical approach to turbulent mixing and chemical reaction Part III computational and experimental results for the new micromixing model, *Chem. Eng. Commun.* 28 (1984) 259–281, <https://doi.org/10.1080/00986448408940137>.
- [38] M.-C. Fournier, L. Falk, J. Villermaux, A new parallel competing reaction system for assessing micromixing efficiency-determination of micromixing time by a simple mixing model, *Chem. Eng. Sci.* 51 (1996) 5187–5192, [https://doi.org/10.1016/S0009-2509\(96\)00340-5](https://doi.org/10.1016/S0009-2509(96)00340-5).
- [39] V.V. Ranade, Modeling of hydrodynamic cavitation reactors: reflections on present status and path forward, *ACS Eng. Au* 2 (2022) 461–476, <https://doi.org/10.1021/acseengineeringau.2c00025>.
- [40] J.H.A. Schuurmans, M. Peeters, M. Dorbec, K.P.L. Kuijpers, Determination of micromixing times in commercially available continuous-flow mixers: evaluation of the incorporation and interaction by exchange with the mean model, *J. Flow Chem.* 14 (2024) 33–42, <https://doi.org/10.1007/s41981-024-00321-4>.
- [41] S.R.L. Gobert, S. Kuhn, L. Braeken, L.C.J. Thomassen, Characterization of milli- and microflow reactors: mixing efficiency and residence time distribution, *Org. Process Res. Dev.* 21 (2017) 531–542, <https://doi.org/10.1021/acs.oprd.6b00359>.
- [42] J.M. Reckamp, A. Bindels, S. Duffield, Y.C. Liu, E. Bradford, E. Ricci, F. Susanne, A. Rutter, Mixing performance evaluation for commercially available micromixers using Villermaux-Dushman reaction scheme with the interaction by exchange with the mean model, *Org. Process Res. Dev.* 21 (2017) 816–820, <https://doi.org/10.1021/acs.oprd.6b00332>.
- [43] X. Guo, Y. Fan, L. Luo, Mixing performance assessment of a multi-channel mini heat exchanger reactor with arborescent distributor and collector, *Chem. Eng. J.* 227 (2013) 116–127, <https://doi.org/10.1016/j.cej.2012.08.068>.
- [44] A.H. El-Shazly, M.G. Fuko, A.G. Sichali, Improving the micromixing and thermal performance using a novel microreactor design, *J. Braz. Soc. Mech. Sci. Eng.* 45 (2023), <https://doi.org/10.1007/s40430-023-04282-y>.
- [45] B.K. Johnson, R.K. Prud'homme, Chemical processing and micromixing in confined impinging jets, *AIChE J.* 49 (2003) 2264–2282, <https://doi.org/10.1002/aic.690490905>.
- [46] E. Schaer, P. Guichardon, L. Falk, E. Plasari, Determination of local energy dissipation rates in impinging jets by a chemical reaction method, *Chem. Eng. J.* 72 (1999) 125–138.
- [47] Q. Chen, Y. Wang, C. Du, J. Deng, G. Luo, Micromixing performance of a miniaturized annular rotating flow mixer (MARFM), *Chem. Eng. Process. - Process Intensif.* 182 (2022), <https://doi.org/10.1016/j.cep.2022.109181>.
- [48] Z. Zhang, H. Xue, W. Liu, W. Zhao, Z. Chen, Q. Chen, D. Wang, J. Ji, Micromixing in a novel microannular rotating bed, *Ind. Eng. Chem. Res.* 63 (2024) 1321–1333, <https://doi.org/10.1021/acs.iecr.3c03717>.
- [49] D. Wang, Y. Qiu, Z. Chen, C. Gu, X. Ling, H. Peng, X. Yang, F. Yuan, J. Du, W. Yu, Characterization of micromixing intensification of impinging jet flow on a spinning disk reactor with a structured surface, *Ind. Eng. Chem. Res.* 63 (2024) 10782–10794, <https://doi.org/10.1021/acs.iecr.4c01059>.
- [50] A. Gode, A.H. Thaker, V.V. Ranade, Comparison of devices used for continuous production of emulsions: droplet diameter, energy efficiency and capacity, *Chem. Eng. Process. - Process Intensif.* 203 (2024), <https://doi.org/10.1016/j.cep.2024.109881>.
- [51] K. Madane, V.V. Ranade, Anti-solvent crystallization: particle size distribution with different devices, *Chem. Eng. J.* 446 (2022), <https://doi.org/10.1016/j.cej.2022.137235>.
- [52] C. Baqueiro, N. Ibaseta, P. Guichardon, L. Falk, Influence of reagents choice (buffer, acid and inert salt) on triiodide production in the Villermaux-Dushman method applied to a stirred vessel, *Chem. Eng. Res. Des.* 136 (2018) 25–31, <https://doi.org/10.1016/j.cherd.2018.04.017>.
- [53] D. Wenzel, M. Assirelli, H. Rossen, M. Lopatshchenko, A. Górak, On the reactant concentration and the reaction kinetics in the Villermaux-Dushman protocol, *Chem. Eng. Process. - Process Intensif.* 130 (2018) 332–341, <https://doi.org/10.1016/j.cep.2018.06.022>.
- [54] P. Guichardon, L. Falk, J. Villermaux, Characterisation of micromixing efficiency by the iodide-iodate reaction system. Part II: kinetic study, *Chem. Eng. Sci.* 55 (2000) 4245–4253.
- [55] G. Schmitz, Kinetics and mechanism of the iodate-iodide reaction and other related reactions, *PCCP* 1 (1999) 1909–1914, <https://doi.org/10.1039/a809291e>.
- [56] R. David, J. Villermaux, Interpretation of micromixing effects on fast consecutive-competing reactions in semi-batch stirred tanks by a simple interaction model, *Chem. Eng. Commun.* 54 (1987) 333–352, <https://doi.org/10.1080/00986448708911913>.
- [57] L. Falk, J.M. Commenge, Performance comparison of micromixers, *Chem. Eng. Sci.* 65 (2010) 405–411, <https://doi.org/10.1016/j.ces.2009.05.045>.
- [58] J. Carpenter, M. Badve, S. Rajoriya, S. George, V.K. Saharan, A.B. Pandit, Hydrodynamic cavitation: an emerging technology for the intensification of various chemical and physical processes in a chemical process industry, *Rev. Chem. Eng.* 33 (2017) 433–468, <https://doi.org/10.1515/revce-2016-0032>.
- [59] P. Senthil Kumar, M. Siva Kumar, A.B. Pandit, Experimental quantification of chemical effects of hydrodynamic cavitation, *Chem. Eng. Sci.* 55 (2000) 1633–1639.
- [60] N.P. Vichare, P.R. Gogate, A.B. Pandit, Optimization of hydrodynamic cavitation using a model reaction, *Chem. Eng. Technol.* 23 (2000) 683–690, <https://doi.org/10.1002/1521-4125>.
- [61] J. Baldyga, J.R. Bourne, *Turbulent Mixing and Chemical Reactions*, Wiley, 1999.
- [62] R.S. Abiev, I.V. Makusheva, A.I. Mironova, Comparison of hydrodynamics and micromixing quality in a two-stage microreactor with intensely swirled flows and in a T-mixer, *Chem. Eng. Process. - Process Intensif.* 202 (2024), <https://doi.org/10.1016/j.cep.2024.109829>.
- [63] C.M. Khalde, A.V. Pandit, J.S. Sangwai, V.V. Ranade, Flow, mixing, and heat transfer in fluidic oscillators, *Can. J. Chem. Eng.* 97 (2019) 542–559, <https://doi.org/10.1002/cjce.23377>.
- [64] K. Madane, V. Ranade, Jet oscillations and mixing in fluidic oscillators: influence of geometric configuration and scale, *Ind. Eng. Chem. Res.* 62 (2023) 19274–19293, <https://doi.org/10.1021/acs.iecr.3c02077>.

- [65] A. Simpson, V.V. Ranade, Flow characteristics of vortex based cavitation devices: computational investigation on influence of operating parameters and scale, *AIChE J.* 65 (2019), <https://doi.org/10.1002/aic.16675>.
- [66] S. Song, Z. Liu, L. Guo, W. Yao, H. Liu, M. Yang, G. Chen, Continuous and size-control of lipopolyplex nanoparticles enabled by controlled micromixing performance for mRNA delivery, *J. Flow Chem.* 14 (2024) 451–468, <https://doi.org/10.1007/s41981-024-00316-1>.
- [67] J. Gradl, W. Peukert. Characterization of Micromixing for Precipitation of Nanoparticles in a T-Mixer, in: H. Bockhorn, D. Mewes, W. Peukert, H. J. Warnecke (Eds.), *Micro and Macro Mixing. Heat and Mass Transfer*, Springer, 2010.